Aging reduces motivation through decreased *Bdnf* expression in the ventral tegmental area

Hanyue Cecilia Lei[1], Kyle E. Parker[2], Carla M. Yuede[3],
Jordan G. McCall[2]*†, Shin-ichiro Imai[1]*†

[1]Department of Developmental Biology, Washington University School of Medicine; Saint Louis, Missouri, USA.

[2]Department of Anesthesiology, Washington University School of Medicine; Saint Louis, Missouri, USA.

[3]Department of Psychiatry, Washington University School of Medicine; Saint Louis, Missouri, USA.

*Shin-ichiro Imai. Email: imaishin@wustl.edu

*Jordan G. McCall. Email: jordangmccall@wustl.edu

†Equally contributing authors

Abstract:

Age-associated reduced motivation is a hallmark of neuropsychiatric disorders in the elderly. In our rapidly aging societies, it is critical to keep motivation levels high enough to promote healthspan and lifespan. However, how motivation is reduced during aging remains unknown. Here, we used multiple mouse models to evaluate motivation and related affective states in young and old mice. We also compared the effect of social isolation, a common stressor, to those of aging. We found that both social isolation and aging decreased motivation in mice, but that *Bdnf* expression in the ventral tegmental area (VTA) was selectively decreased during aging. Furthermore, VTA-specific *Bdnf* knockdown in young mice recapitulated reduced motivation observed in old mice. These results demonstrate that maintaining *Bdnf* expression in the VTA could promote motivation to engage in effortful activities and potentially prevent age-associated neuropsychiatric disorders.

In 2017, the World Health Organization reported that more than 20% of people aged 60 and over have a psychiatric or neurological disorder, including dementia, depression, and anxiety (1). Older adults are also more susceptible to stressors such as social isolation, a common risk factor for many mental disorders and health issues particularly during the ongoing COVID-19 pandemic (*2-4*). These age-associated psychiatric conditions are quite often associated with reduced motivation to engage in effortful activities (*5*). Furthermore, maintaining high motivation levels is indicative of healthy mental conditions in old age (*6*). However, how aging affects mental functions, particularly motivation, as well as the underlying biological mechanisms, remains largely unknown.

To determine the neurobiological mechanisms of aging-induced decreased motivation, we adapted multiple mouse models thought to impact motivation. Particularly, we used social isolation as a stressor to mimic a real-life condition in aging human population (*7, 8*). We used sexually matured young adult (4 month-old) and old but still healthy (18 month-old) male mice. After one month of single or grouped housing, these mice were examined in a battery of motivational assays.

Voluntary wheel-running activity (VWR) is innately rewarding to rodents even with no other extrinsic reward (*9, 10*). Therefore, to test whether age impacts this endogenously motivated behavior, we compared VWR activities between young and old mice under grouped housing or social isolation. Old mice ran much less than young mice during the dark time, as reported previously (*11, 12*). However, social isolation substantially reduced dark-time wheel-running in both young and old mice (Fig. 1, A and B). Most VWR reduction occurred in the early dark time when mice reached their daily peaks of running (fig. S1, A and B), and the effect of social isolation was greater in old mice, compared to young mice (40.3% vs. 25.7% reduction). Although VWR is a complex behavior that can be affected by both physiological (e.g., reduced skeletal muscle strength and energy metabolism) and motivational changes, these results imply that both aging and social isolation undermine motivation.

To directly examine whether aging and social isolation reduce motivation levels in mice, we next conducted an operant progressive ratio (PR) test to measure the amount of effort that animals are willing to expend to gain a palatable food reward. We habituated mice to sugar pellets in home cages two days before training and trained under fixed ratio 1 and fixed ratio 3 for five days each (fig. S1C). Following this task learning, we next tested the mice under a progressive ratio (PR) for one day (Fig. 1C). In the PR test, socially isolated young mice performed significantly fewer correct nose-pokes than group-housed controls (Fig. 1D). Interestingly, group-housed old mice showed significantly lower correct nose-pokes than group-housed young mice, but very similar to those of the socially isolated young mice (Fig. 1D). Socially isolated old mice tend to show further reduction in correct nose-pokes (Fig. 1D). Breakpoint analysis, which determines the maximum number of nose-pokes that an animal achieves to gain a single reward, further demonstrates consistent reduction in effort to achieve rewards in old and socially isolated mice (Fig. 1E). In both socially isolated groups, there were tendencies of fewer entries into the food tray (fig. S1D). These results clearly suggest that reduced motivation is a shared outcome of social isolation and aging, and old mice seemingly responded less to the stress of social isolation perhaps due to the already reduced effort induced by aging.

Apathy and anhedonia are often comorbid with decreased motivation (*13*). To determine whether normal reward processing is impacted by social isolation and aging, we next conducted the sucrose preference test (SPT). All groups of mice manifested robust preference to sucrose

solution over water in the sucrose preference test (fig. S1E), indicating no obvious anhedonia. Nonetheless, the amount of sucrose solution consumed was selectively reduced by social isolation and aging (Fig. 1F), although the extent of reduction by social isolation did not reach statistical significance in either young or old mice. Reduction in energy demand was an unlikely explanation because daily food intakes of all four groups on the test day were not different (fig. S1F). Notably, the results from the SPT showed very similar patterns to those from the PR test, supporting the notion that social isolation and aging both reduce motivated behavior in mice.

Finally, to determine whether approach-avoidance conflicts that underly some features of an anxiety-like state might be altered by social isolation and aging in young and old mice, we tested mice in the open field test (OFT) and elevated plus maze (EPM). Socially isolated young mice spent less time exploring the center area than the group-housed controls, whereas both group-housed and socially isolated old mice exhibited similarly lowered center time (Fig. 1G). Additionally, in the EPM, social isolation increased travel distances and percentages of moving times in the close arm in both young and old mice, as we observed previously (*14*), whereas there were no differences between young and old mice (fig. S2, A to C). Therefore, when motivation was reduced by social isolation and aging, certain anxiety- or depression-related behavioral states were also present. Together, these results suggest that aging and social isolation both reduce motivation, but perhaps not additively.

To determine the extent to which age alters motivation, we tested a new cohort of young and old mice across different testing conditions. Remarkably, we found that when food-deprived and tested during the dark time (Fig. 2A), differences in correct nose-pokes detected in the PR test between young and old mice were greatly enhanced (Fig. 2B). Consistent results were obtained for break points (Fig. 2C). These results suggest that the reward-seeking motivation of young mice is enhanced by fasting and heightened during the dark time, whereas old mice fail to show such dark time-dependent enhancement of reward-seeking motivation, confirming that aging is a critical contributor to reduced motivation.

Extensive literature has defined the role of the mesolimbic dopamine (DA) system in regulating reward and motivation (*15, 16*). Two major DA populations are identified in the ventral tegmental area (VTA) and the substantia nigra (SN) that locate adjacently in the ventral midbrain (*17*). To determine the mechanism for this age-associated decline in motivation, we examined mRNA expression levels of characteristic functional genes in these two regions by collecting tissue samples from young and old brain sections with laser-capture microdissection and conducting quantitative RT-PCR. We found that expression of brain-derived neurotrophic factor (*Bdnf*) was significantly decreased in the aged VTA (Fig. 3A). Interestingly, genes related to DA turnover did not show any significant changes. The expression of *Gria1*, which encodes the GluA1 AMPA glutamate receptor subunit, tended to decrease in aged VTA (Fig. 3A). On the other hand, no genes examined in the SN were significantly altered during aging, except for a trend of increase in the expression of *Maoa*, which can be indicative for augmented DA metabolism and oxidative stress in this region (Fig. 3B) (*18, 19*). We also confirmed this age-associated decrease in *Bdnf* expression by fluorescent *in situ* hybridization. Lower *Bdnf* signals were detected across eight consecutive bregma levels throughout the aged VTA, compared to the young VTA, whereas the expression of *Slc6a3*, a DA neuronal marker, did not show any significant differences between young and old mice (Fig. 3, C to G). Age-associated decreased *Bdnf* expression was present throughout the VTA in both *Slc6a3*-positive and *Slc6a3*-negative cells (fig. S3, A to D), suggesting widespread downregulation of *Bdnf* throughout the VTA. Whereas aging selectively decreased *Bdnf* expression in the VTA, social isolation did not

decrease *Bdnf* expression in the VTA (fig. S3E, left panel). On the other hand, social isolation tended to decrease *Bdnf* expression in the dorsal raphe nucleus (DRN) at least in young mice (fig. S3E, right panel). Given that the activity of DRN DA neurons is important to elicit a loneliness-like state and promote social preference (*20*), a commonality between aging and social isolation is decreased *Bdnf* expression, but in different areas of the brain.

Following the observation that VTA *Bdnf* was decreased in aged mice, we next sought to determine whether decreasing VTA *Bdnf* expression in young mice can recapitulate the motivational dysfunction observed in aged mice. To do so, we knocked down *Bdnf* expression in the VTA by stereotactically injecting a *Bdnf* shRNA-expressing lentivirus into the VTA of young mice. Two months after surgery, the VTA-specific *Bdnf*-knockdown (VTA-*Bdnf*-KD) mice were tested for the extended PR paradigm with food deprivation during light and dark times (Fig. 4, A to C). Importantly, VTA-*Bdnf*-KD mice exhibited significant reduction in correct nose-pokes and break points with food deprivation during both light and dark times, successfully recapitulating motivational phenotypes observed in aged mice (Fig. 4, D and E, and fig. S4, A and B). On the other hand, VTA-*Bdnf*-KD mice did not alter behaviors in the VWR and OFT (Fig. 4, F to I, and fig. S4, C and D), supporting a selective role of *Bdnf* in the VTA in reward-seeking motivational behavior. Taken together, these results demonstrate that specific decreases in *Bdnf* expression in the aged VTA contribute, at least in part, to age-associated reduced motivation in mice.

Here we demonstrated that both social isolation and aging significantly decreased motivation in mice along with the induction of certain anxiety- or depression-related behaviors. Aging is a strong contributor to reduced motivation, and this may explain why aged mice respond substantially less to social isolation compared to young mice. In this regard, we found that *Bdnf* expression was significantly reduced throughout the aged VTA, in both DA and non-DA cells. Remarkably, the VTA-specific knockdown of *Bdnf* in young mice recapitulated the reduced motivation observed in old mice, suggesting that this VTA-specific reduction in *Bdnf* contributed to the impaired reward-seeking motivation in aged mice. Whereas VTA BDNF levels have been implicated in the development and progression of drug-induced reward processing or addiction (*21, 22*), our findings suggest that BDNF also plays an important role in maintaining motivated states in a healthy, physiological condition, which we showed impaired with age. Importantly, while the high frequency of depression in Parkinson's disease appears dependent on decreased DA innervation of the limbic system (*23, 24*), the age-associated decreases we observed in VTA *Bdnf* expression occurred in both DA and non-DA cells, suggesting that this is a distinct mechanism for age-associated decreased motivation. Interestingly, it has been reported that leptin receptor-expressing neurons in the lateral hypothalamus (LH) mainly project to non-DA VTA neurons and drive PR performance through the activation of these VTA neurons (*25*). We previously showed that specific neuronal populations in the dorsomedial hypothalamus and LH play critical roles in counteracting age-associated functional decline and determining longevity in mice (*26, 27*). Therefore, it will be of great interest to determine whether these neuronal populations that fundamentally control aging and longevity also regulate motivation through *Bdnf*-expressing VTA neurons. Because the LH shows significant reduction in its NAD^+ levels during aging and may rely on extracellular nicotinamide phosphoribosyltransferase (eNAMPT), an important NAD^+ biosynthetic enzyme counteracting aging, for its NAD^+ biosynthesis (*28-30*), it will be of great importance to examine whether eNAMPT supplementation could restore motivation in aged mice. In conclusion, our study advances our understanding for the mechanism of age-associated motivational changes and stimulates development of interventions to keep our motivation levels high and healthy.

Materials and Methods

Animals

All animal procedures were approved by the Washington University Institutional Animal Care and Use Committee and were in accordance with National Institutes of Health guidelines. Unless otherwise noted, all mice were housed in groups of 3-5, fed *ad libitum* on a standard chow diet (PicoLab Rodent Diet 20-5053; LabDiet, St. Louis, MO) and autoclaved water in a temperature/humidity-controlled holding room within a barrier facility, maintained on a 12:12-hr light/dark cycle. Food, beddings (Aspen Chip, Northeastern Products Corp.), and nesting material (Nestlets, Ancare) were changed once per week; water bottles were changed as needed. Mice were labeled on their tails with sharpie markers for easy identification and monitored constantly for their health status. All handling, cage changing, measuring procedures, and behavior tests were conducted by the same experimenters throughout the study. Only male mice were used.

All aged mice and the corresponding young groups were obtained from the NIH aged rodent colony (C57BL/6JN); All group-housed cages were housed only with original cage mates from weaning. Mice used for *Bdnf* knock-down analysis were purchased from Jackson Laboratories (C57BL/6J) at 12-week-old and acclimated to the animal facility for ~2 months before surgeries; upon arrival, mice were randomly assigned into cages of 4/5 and maintained until sacrifice.

Social isolation procedure

All mice were originally group-housed in cages of 3-5 cage mates. After acclimation to the holding rooms, cages containing around half of the animals were separated into individual cages and maintained isolated until sacrifice; the rest of the control cages were remained unchanged across the study. All cages within a certain cohort were placed in proximity on the same rack to control for traffic, noise levels, and light exposure.

Behavior tests

All behavioral tests were performed within a sound-attenuated room maintained at 20-26°C after at least one week of acclimation to the local holding room. All tests were performed by female experimenters. Unless otherwise noted, all mice in the same cohort underwent the same test/procedure on the same day(s) from ZT3 to ZT9; if a test/procedure cannot be finished within one day, the cohort will be divided into sub cohorts by counterbalancing grouping, home cages, and other factors. For all experiments performed outside of the holding room, mice were brought into the corresponding behavior space to habituate for at least 20 minutes before any test/procedure started. All behavioral apparatuses were cleaned with 2% chlorhexidine in between subjects.

Operant Progressive-Ratio Test

To expose the animals to the reward, mice fed *ad libitum* were given 3 g/mouse of the reward sugar pellet (Dustless Precision Pellet, F0071, Bio-Serv) on the bedding of their home cages when cages were changed at ZT12. Consumption of the pellets was confirmed the next day. One day after the exposure, mice were gently placed in a mouse operant-conditioning box (15.24×13.34×12.7 cm) within a sound attenuating cubicle (ENV-307A & ENV-020M, Med Associates Inc., Fairfax, VT). The box was equipped with a stainless steel grid floor, two nose holes (active and inactive) flanking a trough pellet receptacle (food tray) connected to a pellet

dispenser on the bottom of the right-hand side wall; a house light was installed at the top center of the left-hand side wall. Pokes into the ports are monitored by infrared light beam sensors. Upon starting of a fixed-ratio 1 (FR1) session, both nose holes present a cue light; one nosepoke into the active hole results in a sugar pellet (20 mg) dispensed to the food tray, along with cue lights turned off and house light turned on for 2 s, during which no action triggers event (time-out period); poking the inactive hole has no consequence. Each session lasted 60 minutes. In between trials, boxes were cleaned with 2% chlorhexidine, and leftover pellets in the dispenser were replaced with fresh and intact ones. All trials took place from ZT3 to ZT8, unless otherwise specified, and each animal was subjected to the sessions at the same time across days. In FR1, mice were trained to discriminate the active hole from the inactive one and receive rewards from the food tray. Following 5 consecutive days of FR1 sessions, mice were moved on to another 5 consecutive days of 60-min fixed-ratio 3 (FR3) sessions, in which three active nosepokes results in one reward delivery and 20 s time-out period. Mice were conditioned to repeatedly perform the correct operant behavior until receipt of the reward during FR3. After completion of the training, motivation levels of the mice were assessed using a progressive-ratio (PR) schedule of reinforcement following the equation: response ratio = $5e^{reward\ number/5} - 5$ (rounded to the nearest integer), resulting in an exponential increase of the number of correct pokes required for each subsequent reward: 1, 2, 4, 7, 9, 12, 15, 20, 25, 32, 40, 50, 62, 77, 95, 118, 145, 178, 219, 268, 328, 402… (*31*). All events were programed, and actions were recorded using MED-PC software (Med Associates) controlled by a PC. The number of active nosepokes counted toward rewards during the 60-min session was calculated as the readout of motivation; A break point (BP) was calculated by taking the bigger number of the last completed ratio versus the number of correct nosepokes after the last reward (*32*). For the extended PR paradigm, following FR1 and FR3 training, two PR sessions were conducted on consecutive days, and the averaged readouts served as the PR baseline. Mice then underwent a break day with no session, followed by a third PR test (light fed) under the same conditions (*ad libitum* in the light time); after another break day and overnight fasting from ZT12, a fourth PR test was conducted (light fasted); lastly, two days after, the mice were fasted from ZT0, and a fifth PR test under fasting was conducted during ZT15-20 under dim red lighting (~10 Lux).

Sucrose Preference Test

Mice were habituated to the sipper tubes in their original home cages by replacing the drinking bottle with a sipper tube for 4 days; daily water consumption was confirmed to be > 2 mL/mouse/day by the last day of the habituation. The sipper tube was home-constructed with a cut 25-ml plastic serological pipettes and a stainless steel pin valve (Lixit) sealed together with heat shrink tubing. Mice were then all separated into individual cages (if not already separated as part of the social isolation procedure), given *ad libitum* regular chow and two identical sipper tubes positioned side-by-side next to the chow, both containing drinking water. Baseline water consumption was measured by recording volume left in each sipper tube daily for 4 days. After that, water in one of the tubes was replaced with 2% sucrose solution. Sucrose solution and water consumed per day were recorded for another 4 days, and the percentage of sucrose solution over total liquid intake was calculated to represent sucrose preference. Tube positions (left vs right) were switched daily after volume checking across the entire test. Mice were housed back with their original cage mates after the procedure was finished.

Elevated-Plus Maze Test

The EPM was performed under dim warm lighting stabilized at ~5-6 lux. The apparatus was a plus-shaped platform comprised of two open arms (25×5×0.5 cm) across from each other and perpendicular to two closed arms (25×5×16 cm) with a center platform (5×5×0.5 cm), elevated to be 50 cm above the floor (60140, Stoelting Co). After habituating to the room, each mouse was individually placed onto the apparatus from one of the open arms and allowed to freely explore. Activity was video recorded using a CCD camera for 20 minutes and videos analyzed using Ethovision XT 13 (Noldus Information Technology, Wageningen, The Netherlands). Behavior tracking after the mice made the first entry into the center area was included in the analysis.

Open Field Test

The OFT was performed under dim warm lighting stabilized at ~5-6 lux. The apparatus consisted of an open-top opaque square enclosure (50×50×31 cm). After habituating to the room, each mouse was individually placed in the center of the apparatus and allowed to freely explore. Activity was video recorded using a Google Pixel 3 XL smartphone for 30 minutes and videos analyzed using Ethovision XT 13. The center was defined as a square comprised of 36% the total area of the OFT (i.e., each side was 0.6 that of the total arena).

One-hour Locomotor Activity and Open Field Test

The 1-hour LA/OFT was conducted in the Animal Behavior Core at Washington University School of Medicine in St. Louis. The test was performed under standard room lighting stabilized at ~150 lux The apparatus consisted of a transparent (40.6×40.6×38.1 cm) polystyrene enclosure, surrounded by a frame containing a 16×16 matrix of photocell pairs. Output was fed to an online computer and analyzed by the system software (Hamilton-Kinder, LLC, Poway, CA). A center area was defined as a 9x9 grid within the 15x15 grid in this chamber, with the peripheral area extending to the sides of the chamber as the outermost boundary. After habituating to the room, each mouse was individually placed in the center of the apparatus and allowed to freely explore for one hour.

Voluntary wheel-running activity

After concluding prior behavior test(s), mice were transferred to the VWR facilities and housed individually in a Tecniplast polycarbonate cage (33.2×15×13 cm) (PT2-MCR, Phenome Technologies) with a vertical running wheel (11 cm inside diameter, 5.4 cm wide), stainless steel wire top, and a filter cage cover (Actimetrics). Wheel-running behavior was recorded and analyzed using Clocklab software (https://actimetrics.com/products/clocklab/). Mice were allowed to habituate to the wheel cages for at least a week and acquire stable running activity before data was collected.

Laser-captured microdissection

Mice were sacrificed by CO_2. Brains were removed, segmented into separate parts in a brain matrix, and immediately embedded in OCT and snap frozen by powered dry ice. Brain samples were stored at −80°C until sliced into 30 um coronal sections in a cryostat at −14°C. Sections were thaw-mounted onto PEN-membrane slides (11505158, Leica Microsystems, Buffalo Grove, IL, USA) and kept frozen until the next step. After collecting all sections containing brain regions of interest, slides were hydrated sequentially in 100%, 95%, 75%, and 50% ethanol for 30 sec each. The hydrated slides were stained with 0.5% Cresyl Violet (Sigma) for 2 min, and

dehydrated with 50%, 75%, 95%, and 2 rounds of 100% ethanol for 30s each. The dehydrated slides were then incubated in xylene twice for 1 min each. After being air-dried, VTA, SN, and DRN regions were microdissected using the Leica LMD 6000 laser-microdissection system, following the Franklin and Paxinos mouse brain atlas. Laser-cut tissue samples were collected in the extraction buffer of the Arcturus PicoPure RNA Isolation Kit (12204-01, Applied Biosystems), and stored at −80°C until RNA was isolated following the manufacturer's protocol and DNase (79254, Qiagen) treatment.

Quantitative real-time RT-PCR

Concentrations of RNA samples were measured by NanoDrop and stored at −80°C until being reverse-transcribed into cDNA with the High Capacity cDNA Reverse Transcription kit (4368814, Thermo Fisher). qRT-PCR was conducted with the TaqMan™ Fast Universal PCR Master mix (4352042, Applied Biosystems) and TaqMan primers for each gene (*Gapdh*: Mm99999915_g1, *Th*: Mm00447557_m1, *Slc6a3*: Mm00438388_m1, *Slc18a2*: Mm00553058_m1, *Ddc*: Mm00516688_m1, *Maoa*: Mm00558004_m1, *Bdnf*: Mm04230607_s1, *Gria1*: Mm00433753_m1) in the StepOnePlus™ Real-Time PCR System (Applied Biosystems). Relative expression levels were calculated for each gene by normalizing to *Gapdh* CT values and then to the mean of the control/reference group.

RNAscope Fluorescent *In Situ* Hybridization (FISH)

Mice were transcardinally perfused first with 0.01 M phosphate-buffered saline (PBS) and then the fixative: 2% paraformaldehyde (PFA) and 0.2% picric acid in 0.01 M PBS, pH 7.4. Brains were removed and post-fixed in the fixative at 4°C overnight, followed by cryoprotection in 20% sucrose in 0.01 M PBS at 4°C for at least 24 hours and snap freezing by powered dry ice. Brains were stored at −80°C until sliced into 20 um coronal sections containing the VTA region in a cryostat at −20°C. Sections were thaw-mounted onto Superfrost™ Plus Microscope Slides (12-550-15, Fisher Scientific) and kept frozen until use. FISH was performed using RNAscope Multiplex Fluorescent Reagent Kit v2 [Advanced Cell Diagnostics, Inc. (ACD)] as per the manufacturer's protocol. Briefly, slides washed with 1x DPBS were fixed in pre-chilled 4% PFA in 1x DPBS at 4°C for 15 min. Sections were then dehydrated through 50%, 70%, and two rounds of 100% ethanol for 5 min each, followed by air-drying. Then the sections were treated with RNAscope® Hydrogen Peroxide for 10 min at room temperature. A hydrophobic barrier was created around the sections using ImmEdge™ Hydrophobic Barrier PAP Pen (H-4000, Vector Laboratories) and allowed to air-dry. The slides were then incubated with Protease III for 30 min and hybridized with ACD probes for target genes (Mm-*Bdnf*-CDS, 457761, probe region 662-1403; Mm-*Slc6a3*-C3, 315441-C3, probe region 1486-2525) for 2 hours at 40°C using a HybEZ™ oven. The signals were amplified by subsequent incubations with Amp-1, Amp-2 and Amp-3 reagents for 30, 30, and 15 min, and then with the HRP reagents, depending on the channels used, in combination with the TSA Plus (NEL760001KT, PerkinElmer) and Opal (FP1487001KT, Akoya) fluorophores at 1:1000 to 1:500 dilutions. Sections were washed with 1x RNAscope Washing Buffer in-between every incubation. Slides were counterstained with DAPI, and coverslips were mounted with FluorSave™ Reagent (345789, Calbiochem). Images were obtained using fluorescent microscopy (DMi8, Leica Microsystems) under 20x magnification. Fluorescent signals were quantified using a customized ImageJ pipeline. Briefly, after tiff images were exported, a circular ROI (radius = 200 um) was selected at the center of the VTA region, referring to the shape covered by the *Slc6a3* signal; after subtracting background

from all channels, the *Slc6a3* channel underwent Gaussian Blur, binary conversion, and shape growth to approximate the area covered by the dopaminergic neurons; the number of the *Bdnf* puncta was quantified using the Find Maxima function, and the identified points were overlayed on the *Slc6a3* area to count the *Bdnf* signals that are expressed in the dopaminergic neurons. For the *Bdnf* knock-down experiment, signals were quantified where the virus caused infection in the VTA.

Virus vector construction

To generate the shRNA expressing lentiviral constructs, 56-bp double-stranded oligonucleotides, each of which contains a sense target sequence, a microRNA based loop sequence (CTTCCTGTCA), an antisense sequence, and a 4-nucleotide sequence complimentary to the vector cutting site of the restriction enzyme AarI at both ends, were generated for *Bdnf* and firefly luciferase (*fLuc*) and cloned into the U6-PGK-GFP vector, provided by the Hope Center Viral Vectors Core at Washington University School of Medicine in St. Louis. Three shRNA targets on the *Bdnf* coding sequence were cloned and tested in parallel, and the one that gave the highest knock-down efficiency *in vitro* was selected for *in vivo* experiments. The sense sequence used for *Bdnf* was 5'-ACTATCCATTCTGGTTGATAA-3' and 5'-TACGCGGAATACTTCGAAATG-3' for *fLuc*. High-titer lentiviruses were produced by the Hope Center Viral Vectors Core. Briefly, HEK293T cells were co-transfected with the shRNA-expressing vectors and three packaging vectors (pMD-Lg/pRRE, pCMV-G, and RSV-REV) by using Polyethylenimine (PEI) reagent. Six hours after transfection, the medium was replaced with the complete medium containing 6 mM sodium butyrate. Culture supernatant was collected 42 hours after transfection. The supernatant was passed through a 0.2 um filter, concentrated by ultracentrifugation through a 20% sucrose cushion, and stored at -80°C until use. Virus titer was determined by transducing HT1080 cells and assaying for vector sequence using qPCR. Virus with titer of 1.1-1.7 x 10^9 IU/ml was used for stereotaxic injection.

Stereotaxic injection

Mice were anaesthetized in an induction chamber (2-4% isoflurane) and placed in a stereotaxic frame (Kopf Instruments, Model 942) where they were maintained under 1-2% isoflurane on a 37°C heating pad throughout the procedure. Following craniotomy under aseptic techniques, mice were injected bilaterally with 1μL of either lenti-shRNA-*Bdnf*-GFP or lenti-shRNA-*fLuc*-GFP at the rate of 200nL/min into the VTA (coordinates relative to Bregma: AP −3.05, ML ± 0.3, DV −4.6), using a Hamilton Neuros Syringe (65460-03, Hamilton), with the beveled opening facing posterior, driven by a Micro4 microsyringe pump controller (World Precision Instruments, Sarasota, FL). The syringe was slowly inserted into the brain tissue and dwelled in place for 3 min before the injection started; after injection, the syringe was dwelled for another 10 min and then slowly withdrawn. The skin incision was closed with 6-0 nylon sutures. Immediately after the surgery, mice were allowed to recover on a heated table (37 °C) until fully awake and then returned to their home cages. All mice in the same cage were injected on the same day. Mice were given Carprofen (Rimadyl) chewable tablet (0.5 mg/mouse/day) as analgesics in home cages for 3 days after surgeries.

Statistical analysis

Data are presented as mean ± standard error of the mean (SEM). Statistical significance was taken as $*P < 0.05$, $**P < 0.01$, $***P < 0.001$ and $****P < 0.0001$, as determined by Student's *t*-

test, Holm-Šídák multiple comparison test, or three-way or two-way repeated-measure ANOVA, followed by post-hoc multiple comparisons as appropriate. Significant and close-to-significance main effects of factors, interactions, and pair-wise comparisons are labeled on the graphs. Sample sizes (N) were determined based on empirical estimations. Data sorting and statistical analysis were performed in R and GraphPad Prism 9.0 (Graphpad, La Jolla, CA).

Illustration and graphing

Graphs are made with GraphPad Prism 9.0. Cartoons are created with BioRender.com and Microsoft PowerPoint.

References and Notes

1. WHO. (World Health Organization, https://www.who.int/news-room/fact-sheets/detail/mental-health-of-older-adults, 2017).
2. Y. Luo, L. C. Hawkley, L. J. Waite, J. T. Cacioppo, Loneliness, health, and mortality in old age: a national longitudinal study. *Soc Sci Med* **74**, 907-914 (2012).
3. C. E. Robb *et al.*, Associations of Social Isolation with Anxiety and Depression During the Early COVID-19 Pandemic: A Survey of Older Adults in London, UK. *Front Psychiatry* **11**, 591120 (2020).
4. K. Sayin Kasar, E. Karaman, Life in lockdown: Social isolation, loneliness and quality of life in the elderly during the COVID-19 pandemic: A scoping review. *Geriatr Nurs* **42**, 1222-1229 (2021).
5. A. Soutschek, A. Bagaini, T. A. Hare, P. N. Tobler, Reconciling psychological and neuroscientific accounts of reduced motivation in aging. *Soc Cogn Affect Neurosci* **17**, 398-407 (2022).
6. M. E. Mortby, A. Maercker, S. Forstmeier, Midlife motivational abilities predict apathy and depression in Alzheimer disease: the aging, demographics, and memory study. *J Geriatr Psychiatry Neurol* **24**, 151-160 (2011).
7. S. Cacioppo, J. P. Capitanio, J. T. Cacioppo, Toward a neurology of loneliness. *Psychol Bull* **140**, 1464-1504 (2014).
8. A. Ieraci, A. Mallei, M. Popoli, Social Isolation Stress Induces Anxious-Depressive-Like Behavior and Alterations of Neuroplasticity-Related Genes in Adult Male Mice. *Neural Plast* **2016**, 6212983 (2016).
9. C. M. Novak, P. R. Burghardt, J. A. Levine, The use of a running wheel to measure activity in rodents: relationship to energy balance, general activity, and reward. *Neurosci Biobehav Rev* **36**, 1001-1014 (2012).
10. J. H. Meijer, Y. Robbers, Wheel running in the wild. *Proc Biol Sci* **281**, (2014).
11. V. Acosta-Rodriguez *et al.*, Circadian alignment of early onset caloric restriction promotes longevity in male C57BL/6J mice. *Science* **376**, 1192-1202 (2022).
12. B. Bartling *et al.*, Sex-related differences in the wheel-running activity of mice decline with increasing age. *Exp Gerontol* **87**, 139-147 (2017).
13. M. Husain, J. P. Roiser, Neuroscience of apathy and anhedonia: a transdiagnostic approach. *Nat Rev Neurosci* **19**, 470-484 (2018).
14. K. E. Parker, J. S. Arackal, S. C. Hunter, J. G. McCall, Punishment Risk Task: Monitoring anxiogenic states during goal directed actions in mice. *bioRxiv*, 2022.2010.2030.514458 (2022).
15. T. N. Lerner, A. L. Holloway, J. L. Seiler, Dopamine, Updated: Reward Prediction Error and Beyond. *Curr Opin Neurobiol* **67**, 123-130 (2021).
16. V. L. Tryon, P. M. Baker, J. M. Long, P. R. Rapp, S. J. Y. Mizumori, Loss of Sensitivity to Rewards by Dopamine Neurons May Underlie Age-Related Increased Probability Discounting. *Front Aging Neurosci* **12**, 49 (2020).
17. Y. Fu *et al.*, A cytoarchitectonic and chemoarchitectonic analysis of the dopamine cell groups in the substantia nigra, ventral tegmental area, and retrorubral field in the mouse. *Brain Struct Funct* **217**, 591-612 (2012).

18. M. Naoi, W. Maruyama, M. Shamoto-Nagai, Type A monoamine oxidase and serotonin are coordinately involved in depressive disorders: from neurotransmitter imbalance to impaired neurogenesis. *J Neural Transm (Vienna)* **125**, 53-66 (2018).
19. S. Raitsin *et al.*, Subchronic glucocorticoids, glutathione depletion and a postpartum model elevate monoamine oxidase a activity in the prefrontal cortex of rats. *Brain Res* **1666**, 1-10 (2017).
20. G. A. Matthews *et al.*, Dorsal Raphe Dopamine Neurons Represent the Experience of Social Isolation. *Cell* **164**, 617-631 (2016).
21. H. Vargas-Perez *et al.*, Ventral tegmental area BDNF induces an opiate-dependent-like reward state in naive rats. *Science* **324**, 1732-1734 (2009).
22. H. Vargas-Perez *et al.*, BDNF signaling in the VTA links the drug-dependent state to drug withdrawal aversions. *J Neurosci* **34**, 7899-7909 (2014).
23. P. Remy, M. Doder, A. Lees, N. Turjanski, D. Brooks, Depression in Parkinson's disease: loss of dopamine and noradrenaline innervation in the limbic system. *Brain* **128**, 1314-1322 (2005).
24. K. R. Chaudhuri, A. H. Schapira, Non-motor symptoms of Parkinson's disease: dopaminergic pathophysiology and treatment. *Lancet Neurol* **8**, 464-474 (2009).
25. F. L. Schiffino *et al.*, Activation of a lateral hypothalamic-ventral tegmental circuit gates motivation. *PLoS One* **14**, e0219522 (2019).
26. A. Satoh *et al.*, Sirt1 extends life span and delays aging in mice through the regulation of Nk2 homeobox 1 in the DMH and LH. *Cell Metab* **18**, 416-430 (2013).
27. N. Ito *et al.*, Slc12a8 in the lateral hypothalamus maintains energy metabolism and skeletal muscle functions during aging. *Cell Rep* **40**, 111131 (2022).
28. M. J. Yoon *et al.*, SIRT1-Mediated eNAMPT Secretion from Adipose Tissue Regulates Hypothalamic NAD+ and Function in Mice. *Cell Metab* **21**, 706-717 (2015).
29. M. Yoshida *et al.*, Extracellular Vesicle-Contained eNAMPT Delays Aging and Extends Lifespan in Mice. *Cell Metab* **30**, 329-342 e325 (2019).
30. S. Johnson, K. Yoshioka, C. S. Brace, S. Imai, Quantification of localized NAD+ changes reveals unique specificity of NAD+ regulation in the hypothalamus. *npj Aging* **In press**, (2023).
31. N. R. Richardson, D. C. Roberts, Progressive ratio schedules in drug self-administration studies in rats: a method to evaluate reinforcing efficacy. *J Neurosci Methods* **66**, 1-11 (1996).
32. V. L. Tsibulsky, A. B. Norman, Methodological and analytical issues of progressive ratio schedules: Definition and scaling of breakpoint. *J Neurosci Methods* **356**, 109146 (2021).
33. S. Sharma, C. Hryhorczuk, S. Fulton, Progressive-ratio responding for palatable high-fat and high-sugar food in mice. *J Vis Exp*, e3754 (2012).
34. R. Weindruch, R. L. Walford, S. Fligiel, D. Guthrie, The retardation of aging in mice by dietary restriction: longevity, cancer, immunity and lifetime energy intake. *J Nutr* **116**, 641-654 (1986).
35. A. Fahlstrom, H. Zeberg, B. Ulfhake, Changes in behaviors of male C57BL/6J mice across adult life span and effects of dietary restriction. *Age (Dordr)* **34**, 1435-1452 (2012).

Acknowledgments: We thank Erik D. Herzog for sharing their wheel-running facility and providing critical suggestions on this study. We also thank members of the Imai lab, particularly Kyohei Tokizane, Cynthia S. Brace, and Brian V. Lananna, and of the Al-Hasani and McCall labs for technical support and valuable discussions. Support was also provided by the Animal Behavior Core (supported in part by the McDonnell Center for Systems Neuroscience and the Taylor Family Institute) and the Hope Center Viral Vectors Core at Washington University School of Medicine.

Funding:

National Institute on Aging grant AG037457 (SI)

National Institute on Aging grant AG047902 (SI)

Washington University School of Medicine Tanaka Fund (SI)

National Institute of Neurological Disorders and Stroke grant NS11789 (JGM)

Brain & Behavior Research Foundation grant NARSAD YI – 28565 (JGM)

LIFENAD Fellowship Fund (HCL)

Author contributions:

Conceptualization: HCL, SI

Experimental design: HCL, KEP, CMY, JGM, SI

Investigation: HCL, CMY

Analysis and interpretation: HCL, KEP, CMY, JGM, SI

Funding acquisition: JGM, SI

Supervision: JGM, SI

Writing – original draft: HCL, SI

Writing – review & editing: KEP, CMY, JGM

Competing interests: S.I. receives a part of patent-licensing fees from MetroBiotech (USA), Teijin Limited (Japan), and Institute for Research on Productive Aging (Japan) through Washington University. S.I. also serves as the President of the Institute for Research on Productive Aging (Japan), and a potential conflict of interest has been properly resolved through the Washington University Conflict of Interest Committee. The other authors have no competing interests to disclose.

Data and materials availability: All data are available in the main text or the supplementary materials.

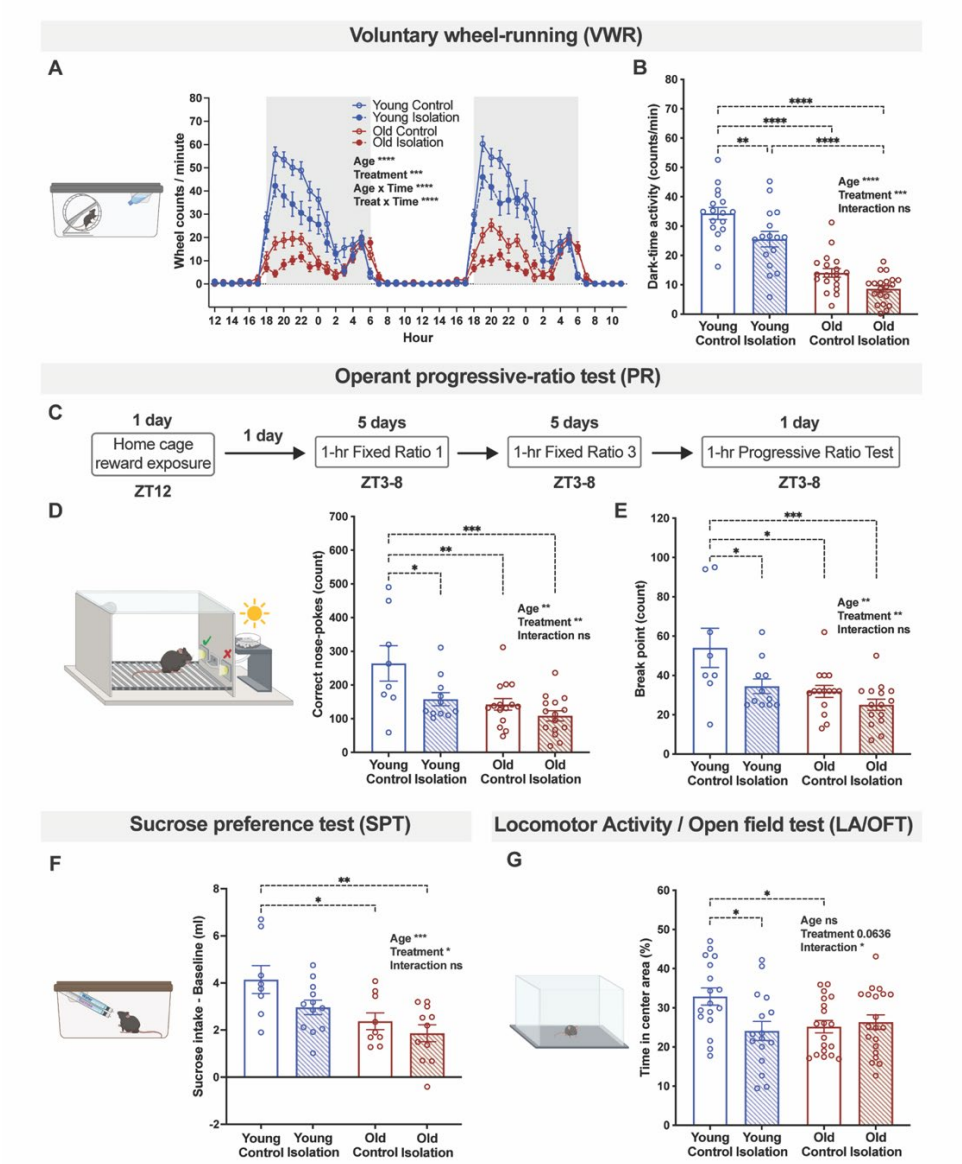

Fig. 1. Chronic social isolation and aging differentially impair motivational behaviors and induce depressive- and anxiety- like behaviors

(**A**) Voluntary wheel-running activity recording in consecutive 48 hours, shaded area representing the dark phase. (**B**) Average VWR activity during the dark phase (ZT12-0). (**C**) Calendar illustrating the operant progressive ratio test protocol. Correct nosepokes performed (**D**) and break points reached (**E**) in the PR test. (**F**) Delta of sucrose solution intake to baseline water intake in the sucrose preference test. (**G**) Percentage of time spent in the center area in the 1-hour locomotor activity and open field test. Data was analyzed by 3-way ANOVA (A) and 2-way ANOVA (B, D, E, F, G) with post-hoc multiple comparisons. N = 7-20. Error bar: SEM. Significant pair-wise comparisons and main effects of factors and interactions are labeled on the graphs: *p≤0.05; **p≤0.01; ***p≤0.001; ****p≤0.0001. Close-to-significance P values are labeled on the graphs.

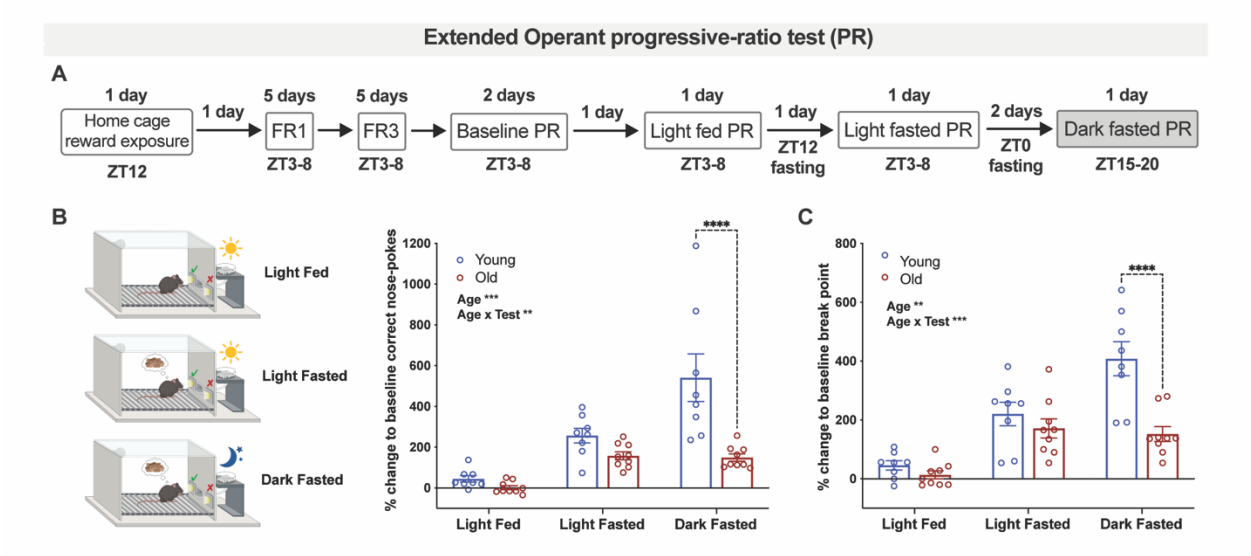

Fig. 2. Aging leads to reduction of fasting-induced motivation for palatable food reward (**A**) Calendar illustrating the extended operant progressive ratio test protocol. Correct nosepokes (**B**) and break points reached (**C**) normalized to individual baseline PR under different experimental conditions in the extended PR. Data was analyzed by 2-way ANOVA with post-hoc multiple comparisons. N = 8/9. Error bar: SEM. Significant pair-wise comparisons and main effects of factors and interactions are labeled on the graphs: *p≤0.05; **p≤0.01; ***p≤0.001; ****p≤0.0001.

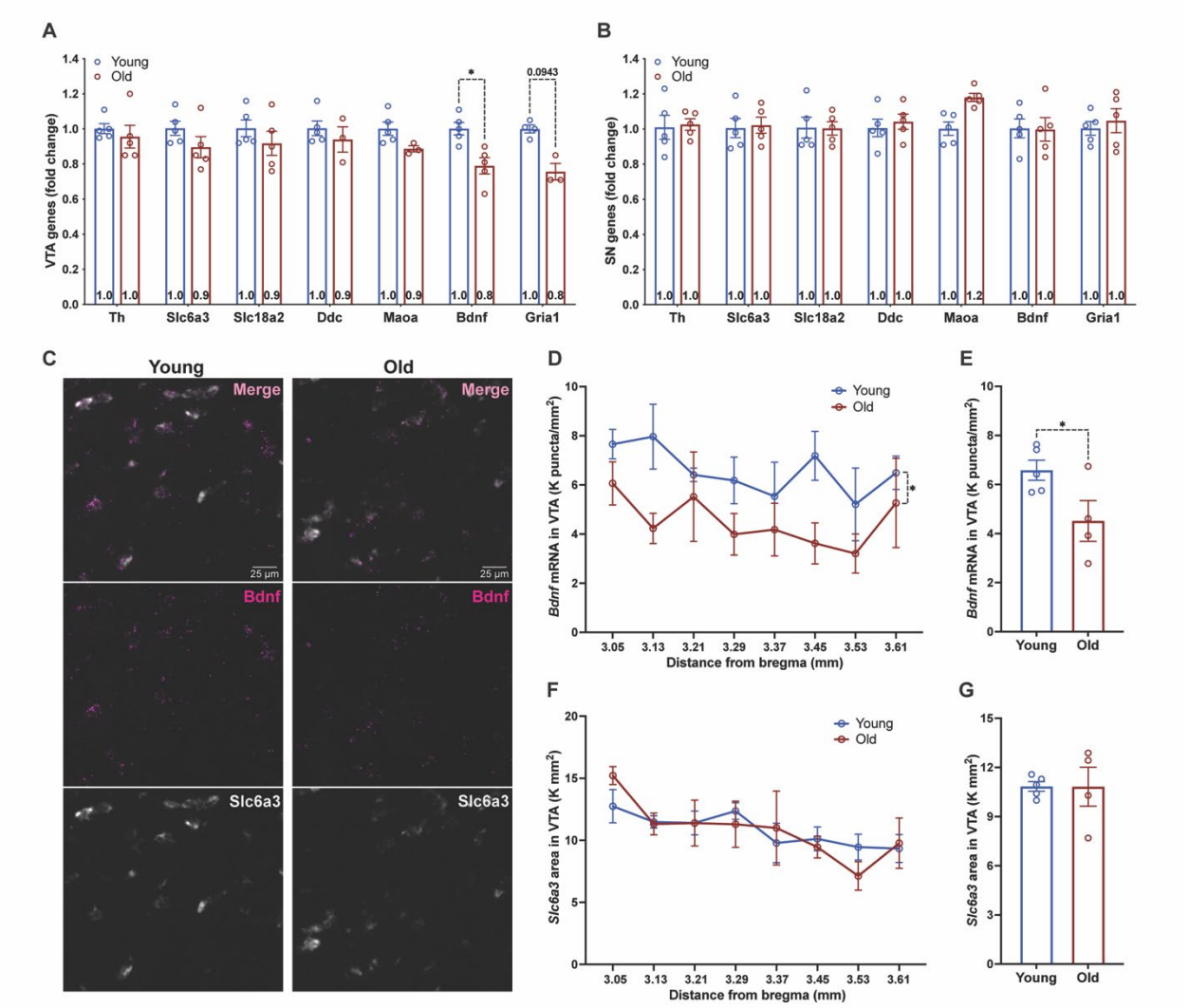

Fig. 3. *Bdnf* gene expression is decreased in the ventral tegmental area (VTA) of aged mice RT-qPCR analysis of laser-capture-microdissected VTA (**A**) and SN (**B**) samples from young and old mice. Representative images of FISH (RNAscope) analysis of *Bdnf* in VTA, using dopamine active transporter (DAT/*Slc6a3*) mRNA as a marker for DA neurons in young vs. old mice are shown in (**C**) and quantified as the density of *Bdnf* mRNA signal puncta in the VTA region (**D**, **E**) and the area of the *Slc6a3* signals (**F**, **G**) in VTA across 8 bregma levels (80µm interval from ~-3.05). *Gria1*: glutamate ionotropic receptor AMPA type subunit 1; *Slc6a3*: solute carrier family 6 member 3. Data was analyzed by 2-way ANOVA with post-hoc multiple comparisons (A, B, D, F) and student's t-test (E, G). N = 3-5. Error bar: SEM. Significant pair-wise comparisons and main effects of factors and interactions are labeled on the graphs: *p≤0.05; **p≤0.01; ***p≤0.001; ****p≤0.0001. Close-to-significance P values are labeled on the graphs.

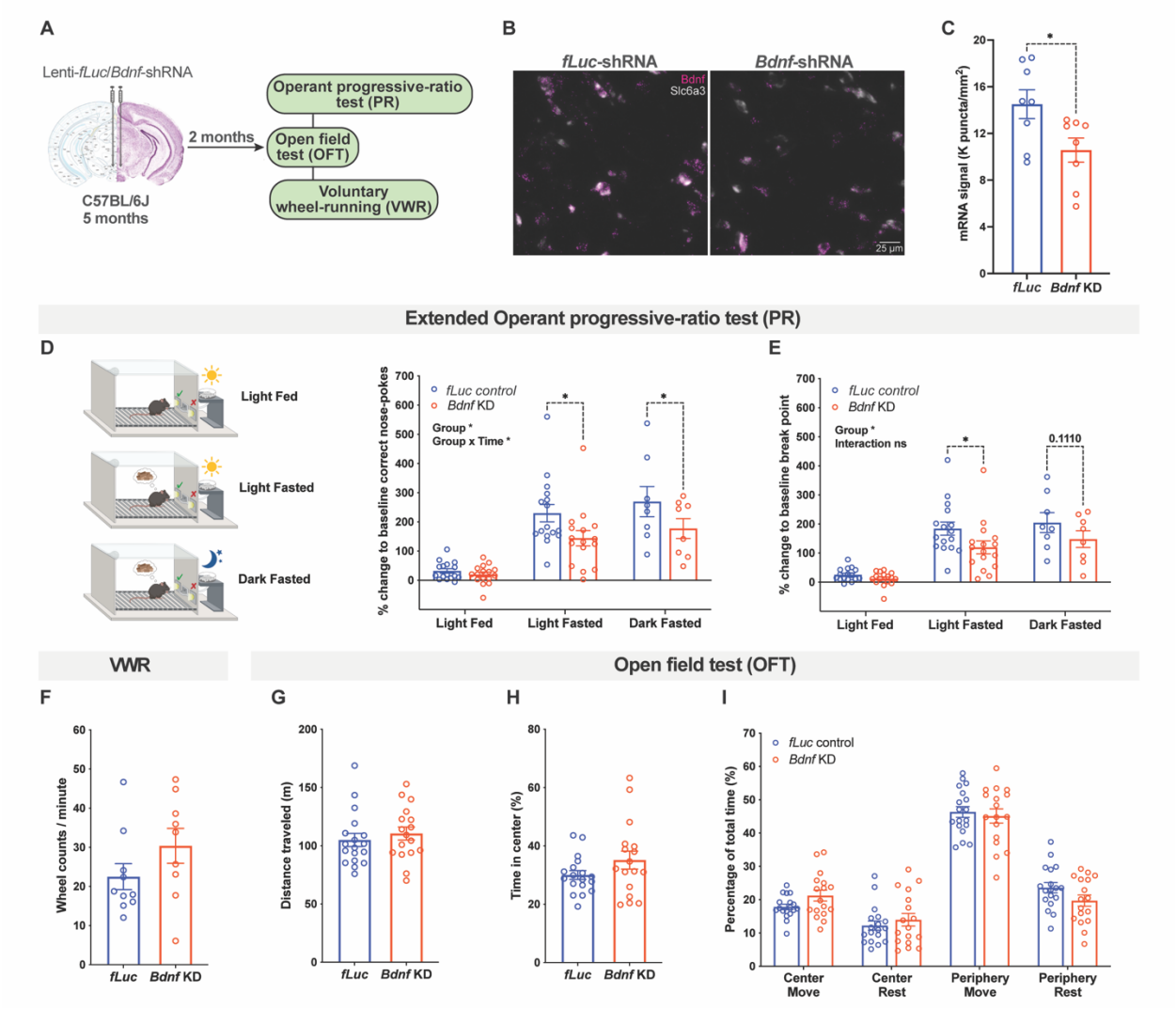

Fig. 4. VTA *Bdnf* KD in young mice partially recapitulates the age-associated reduction in palatable food motivation, not affecting other age-related phenotypes
(**A**) Calendar and schematics illustrating the experimental timeline. (**B**) Representative FISH images of *Bdnf* and Slc6a3 in VTA of *fLuc* vs *Bdnf*-shRNA virus injected mice, (**C**) quantified as the density of *Bdnf* mRNA signal puncta in infected regions (KD efficiency 27%). Correct nosepokes (**D**) and break points reached (**E**) normalized to individual baseline PR under different experimental conditions in the extended PR. (**F**) Average VWR activity during the dark phase (ZT12-0). Total distance traveled (**G**) Percentage of time spent in the center area (**H**) and percentage of time spent moving or resting in the center and peripheral areas (**I**) in the open field test. Data was analyzed by 2-way ANOVA with post-hoc multiple comparisons (D, F), student's t-test (C, F, G, H), and Holm-Šídák multiple comparison test (I). N = 8-18. Error bar: SEM. Significant pair-wise comparisons and main effects of factors and interactions are labeled on the graphs: *p≤0.05; **p≤0.01; ***p≤0.001; ****p≤0.0001. Close-to-significance P values are labeled on the graphs.